Uniform Thermo-Optic Tunability of Dielectric Metalenses

Prasad P. Iyer,[1,*] Ryan A. DeCrescent,[2,*] Tomer Lewi,[1] Nicholas Antonellis,[3] and Jon A. Schuller[1,†]

[1]*Department of Electrical and Computer Engineering, University of California Santa Barbara, USA*
[2]*Department of Physics, University of California Santa Barbara, USA*
[3]*Department of Physics, Wesleyan University, Boston, USA*

(Received 22 February 2018; revised manuscript received 27 April 2018; published 10 October 2018)

The field of low-loss dielectric metasurfaces has created a new paradigm of miniaturization for free-space optical elements. We study the effects of uniformly changing the refractive index of high-index metalenses. We experimentally demonstrate a modal refractive-index change ($\Delta n_{\mathrm{MD}} = 0.15$) in the fundamental Mie resonances in an InSb resonator based on traditional thermo-optic effects. We develop a high aspect ratio metasurface design with simulated 75–90% transmission efficiency and 2π phase shift as a function of cylinder radius. A metalens is shown to have high (>60%) focusing efficiencies for large (up to 0.8) numerical aperture designs. The uniform thermal tuning of the metalens system is studied based on the variations in the spatial phase profile of the individual resonators. We demonstrate that both the operating wavelength ($\Delta\lambda_f = 500$ nm) and the focal length ($\Delta f = 45$ μm) can be dynamically modified based on the chromatic dispersion of the engineered metalens. The results show that static metasurfaces made of high-index semiconductors can be thermally actuated to tune the operating focal wavelength and focal length.

DOI: 10.1103/PhysRevApplied.10.044029

I. INTRODUCTION

Metasurfaces have produced a revolution in the field of optics by enabling unprecedented transformations of the electromagnetic wavefront [1,2]. Dielectric metasurfaces, in particular, can produce arbitrary spatial phase profiles [3] with minimal ohmic losses leading to, e.g., efficient super-oscillatory [4] and axicon [5] lenses and unidirectional beam deflectors [6,7]. Typical meta-optical elements are designed for a specified static function; dynamically tunable metadevices present a principal challenge in the field. Researchers have demonstrated the possibility of reconfiguring metasurface elements using phase change [8,9], thermo-optic [10–12], and free-carrier [13–18] based refractive-index tuning. In these cases, *individual* metasurface elements are tunable [16] or writeable [8], providing great flexibility, but requiring complex addressing schemes. In contrast, *spatially uniform* modulation of metasurface arrays (e.g., through stretchable substrates [19–21] or liquid crystal [22,23] background media) can more easily be implemented and avoids complications arising from, e.g., large spatial gradients and inter-resonator cross-talk [24,25]. However, the effect of uniform index shifts on metasurface functionality has not been described. Recently, the operating wavelengths of static metasurfaces have been extended through judicious design of the chromatic phase dispersion [26,27] of the individual resonator elements of the metasurface to form apochromatic [28] or multi-wavelength [29,30] metalenses. Here, we demonstrate that the refractive-index tunability of dielectric resonators [17] can facilitate a metalens with tunable wavelength and focal length of operation.

To illustrate the fundamental concepts underpinning index-tuned metasurfaces, we begin by demonstrating thermo-optic shifts of single InSb Mie resonators. Single Mie resonators are fabricated using laser-ablation [17] of an InSb wafer to form spheres of required diameter. Using an FTIR spectrometer (VERTEX 70, Bruker) coupled to an infrared microscope (Hyperion 2000, Bruker), we measure the reflection from a single resonator [Fig. 1(a) inset] and normalize that reflection with respect to the substrate. This enables us to uniquely identify the scattering resonances as dips in reflection [17,31]. In Fig. 1(a), each panel shows the reflection spectra from resonators of different sizes demonstrating the geometric dispersion of the fundamental magnetic dipole (MD) and electric dipole (ED) Mie resonances. The MD and ED are eigensolutions to Maxwell's equations for free-space scattering from subwavelength resonators [32], whose resonant (λ_R) conditions are a function of the size (r) and refractive index (n):

$$\frac{nr}{\lambda_R} = \begin{cases} 0.48 \text{ (MD)}, \\ 0.63 \text{ (ED)}. \end{cases}$$

*These authors contributed equally.
†jonschuller@ece.ucsb.edu

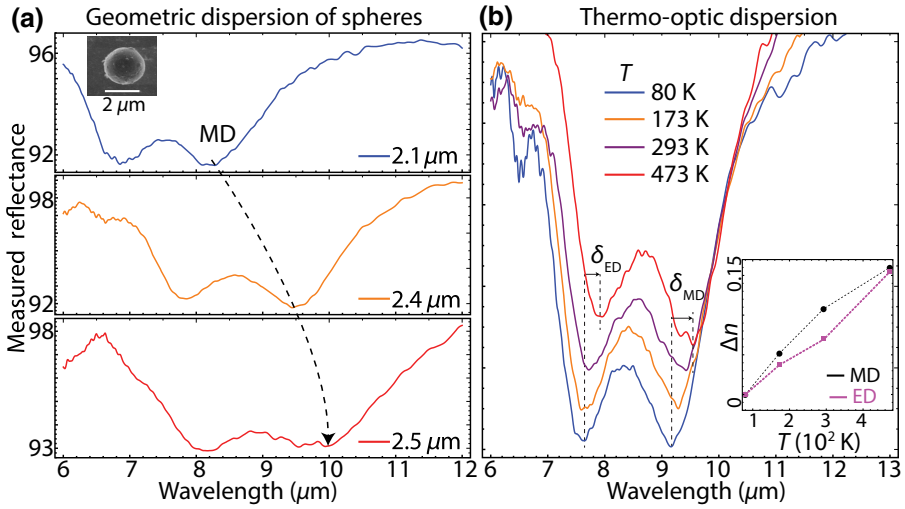

FIG. 1. (a) Fundamental Mie resonances in InSb spheres appear as dips in measured reflectance spectra. The MD resonance dip shifts from 8.15 to 9.75 μm as the diameter of the sphere increases from 2.1 to 2.5 μm. The black arrow indicates this size dependent dispersion of the MD resonance. Inset shows a scanning electron microscope (SEM) image of the 2.1 μm diameter sphere. (b) Spectral shifts of the fundamental Mie resonances due to thermo-optic tuning of the InSb refractive index of a 2.4 μm diameter sphere. The spectra are vertically offset to illustrate the resonant wavelength shift. The refractive-index shift derived from the electric and magnetic dipole spectral resonances is plotted in the inset.

These resonances can be statically tuned by either changing the size [Fig. 1(a)] or dynamically tuned by actively tuning the refractive index of the resonator [Fig. 1(b)]. By changing the temperature, the resonant wavelength from a single antenna can be tuned dynamically from 9.16 to 9.56 μm (7.60–7.89 μm) for the magnetic (electric) dipole resonance. We use the resonant wavelength shift in the magnetic and electric dipole modes to extract the change in the refractive index as plotted in the inset of Fig. 1(b). Traditional thermo-optic shift in InSb increases

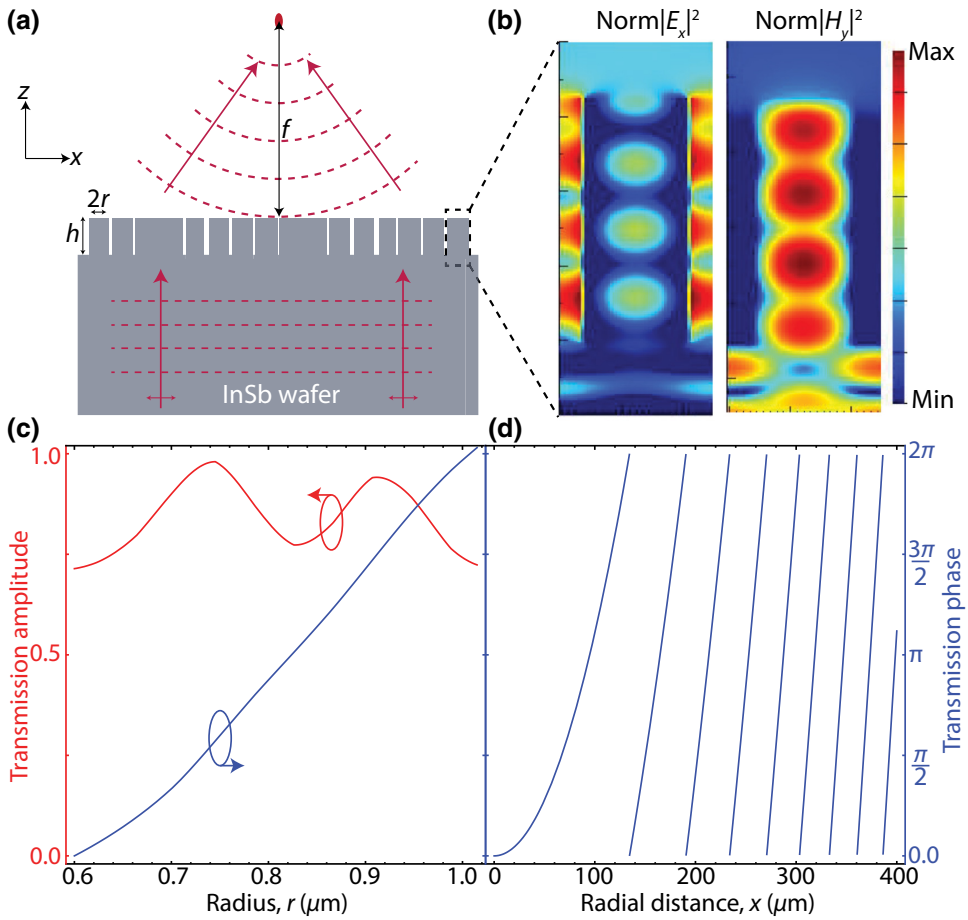

FIG. 2. (a) Schematic of the metalens with a uniform etch depth ($h = 6.5$ μm) and varying cylinder radius focusing a 9-μm plane wave from inside an InSb wafer into free space. (b) Field plots showing the electric and magnetic field intensities at the resonance wavelength within the dielectric resonator. (c) Geometric dispersion in the transmission amplitude (red, left axis) and phase (blue, right axis) of a linearly polarized 9-μm light as a function of cylinder radius. A 2π phase shift with high transmission amplitude of approximately 85% is achieved. (d) The spatial phase function required to convert an incident plane wave into a transmitted focused wave. The spatial phase defined by Eq. (1) is fabricated by choosing the appropriate resonator radius as defined by Fig. 1(c).

the permittivity with temperature due to the bandgap shrinkage, causing the resonant wavelength to redshift [33,34]. At longer wavelengths, thermal free carriers dominate the modal refractive-index change to decrease the effective MD modal index by 0.2 [35] The thermo-optic tuning shown here is common to semiconductors and similar in magnitude to that of, e.g., Ge [33], InAs [33], GaSb [36], and GaAs [36].

To illustrate the effect of a uniform thermo-optic shift, we consider the transmitting metasurface design architecture shown in Fig. 2(a) which consists of an array of high-aspect-ratio cylindrical resonators. We develop a design that requires only a single-step etch of the wafer, making its fabrication process attractive for large-scale implementation. We simulate a cylindrical metasurface lens comprising cylindrical resonators with identical radii along the y axis and variable radii along the x axis (polarization axis) using commercial finite-difference time domain (FDTD) software [37]. Because the resonator and substrate indices are matched, traditional dielectric Huygens metasurface designs [18,38] exhibit neither high transmission nor the 2π phase shifts needed for full phase coverage [35]. Instead, we use high-aspect-ratio cylinders that act like coupled mini-waveguides [39] or higher-order multipolar Mie resonances [32], as evidenced from electric and magnetic field intensities [Fig. 2(b)]. The small spacing between the cylindrical resonators ($d = 2.3$ μm) enables high transmission amplitudes [35] and control of the spatial phase at deeply subwavelength scales. Hence, we can achieve high transmission amplitudes (75–90%) and a 2π phase shift with a cylinder radius [Fig. 2(c)]. The phase addition from each resonator element is designed such that the propagating plane wave in the bulk semiconductor transforms into a spherical wave in free space. The resultant lens design focuses the plane wave of wavelength (λ) in the far field at a focal length (f) based on the spatial phase function:

$$\phi(x) = 2\pi \frac{f}{\lambda}\sqrt{1-\left(\frac{x}{f}\right)^2}. \tag{1}$$

The quadratic spatial phase profile required for this transformation is achieved by changing the radius of the constituent resonators. $\phi(x)$ for focusing a 9-μm incident wave at focal distance (f) of 1 mm is plotted in Fig. 2(d). We simulate a 2-mm-wide aperture with the spatial phase defined by Eq. (1), where the resonator radius at each point on a square grid (2.3-μm periodicity) is chosen based on the calculated size-dependent phase dispersion [Fig. 2(c)]. Ultimately, any spatial phase design can be encoded onto the metasurface using this single-etch resonator system.

We theoretically demonstrate a high-efficiency metalens which focuses a linearly polarized plane wave ($\lambda = 9$ μm) incident from the substrate to a diffraction limited focus [Figs. 3(a) and 3(b)] with a 100-μm focal length. As shown in Fig. 3(c), lenses can be engineered with high (>60%) focusing efficiency (ratio of the power in the main lobe to the total incident power) for a large variation

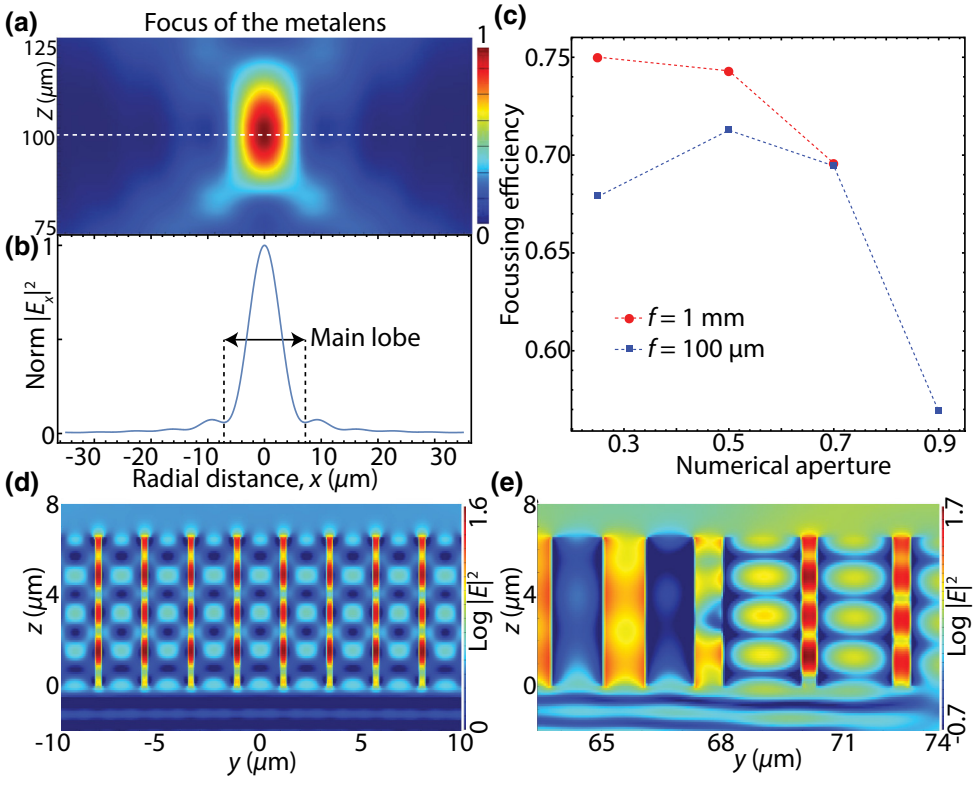

FIG. 3. (a) Electric field intensity at the focus of the metalens simulated with a focal length of 100 μm and N.A = 0.5. (b) Field-intensity line cut taken from Fig. 3(a) (white dashed line). (c) Focusing efficiency of metalenses with two different focal lengths (1 mm in red and 100 μm in blue) at varying NA values. (d),(e) Electric field intensity (in logarithmic scale) in the metalens [Fig. 3(a)] structure at the center (d) and the first phase wrapping region (e) of the metalens, plotted on a logarithmic scale.

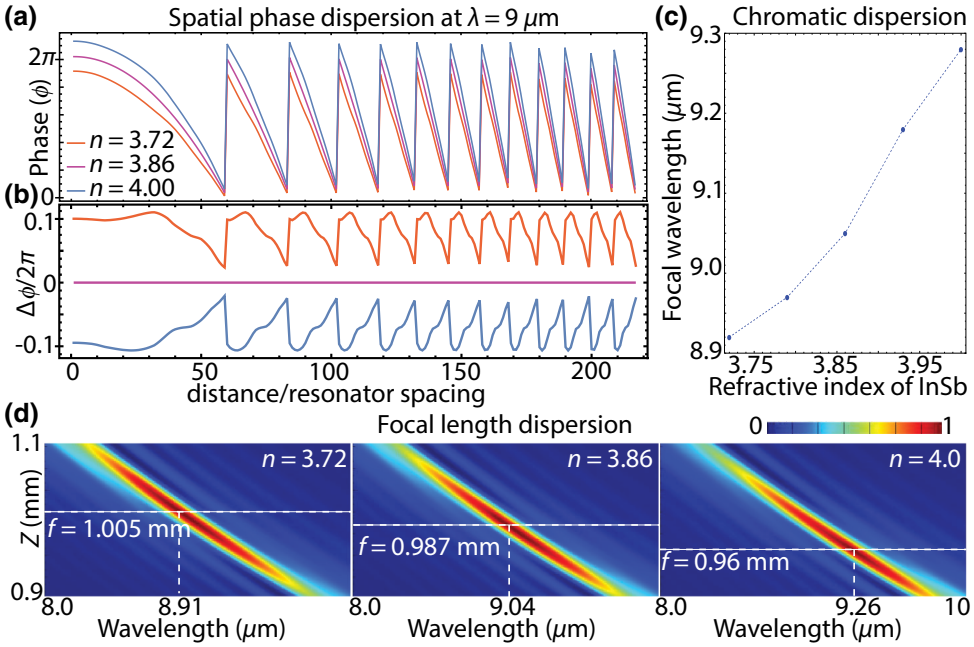

FIG. 4. (a) Variations in the spatial (in units of inter-particle spacing) phase profile of an InSb metalens designed to focus 9-μm infrared light at a -mm focal length for an index of $n_{\mathrm{InSb}} = 3.86$ are shown in pink. Taking the same array dimensions but changing the index to $n = 3.72$ (red) or 4.00 (blue) produces a change in the spatial phase profile. (b) Phase errors ($\Delta\phi$) at the 9-μm operating wavelength when the refractive index is changed to 3.72 (orange line) or 4.00 (blue line) from 3.86 (pink line). Any accumulation of phase error is "reset" due to the 2π phase or radius wrapping of the underlying design. (c) Variation of the focal wavelength—wavelength of highest intensity—as a function of the refractive index. (d) Focal-length dispersion with wavelength for three different metalens refractive indices. The focal wavelength and focal length disperse simultaneously based on the chromatic dispersion of the metalens system.

in focal length (100 μm to 1 mm) and numerical aperture (0.25–0.8). The decreasing focusing efficiency with increasing NA lenses comes from discretization effects at large radial distances due to the quadratically increasing spatial phase. The spatial phase profile for the lens shown in Fig. 3(c) is plotted as the pink line in Fig. 4(a). The lens is designed to operate at 9 μm based on a refractive index of 3.86. The effect of increasing (blue) or decreasing (orange) the index by $\delta n = 0.15$ is also shown in Fig. 4(a). Changing the refractive index causes phase errors that accumulate with distance, but are "corrected" [Fig. 4(b)] every time the resonator radii "reset." The phase wrap from 0 to 2π in the original $n = 3.86$ design causes the resonator radius to transition from the smallest to the largest radius where the accumulated phase error is then eliminated. At a fixed illumination wavelength, the focal length is constant, but the efficiency is expected to decrease due to deviations from the ideal phase function. This behavior can be better understood by examining the chromatic dispersion of the lens at each index value [Fig. 4(d)]. In all cases, the focal distance (i.e., point of maximal intensity at a given wavelength) increases with decreasing wavelength as expected from normal dispersion of diffractive optical elements. This variation is independent of the refractive index. The main effect of changing the index is to change the *optimal* wavelength of operation. Increasing (decreasing) the refractive index increases (decreases) the optimal operating wavelength of the lens [Fig. 4(c)], mirroring the Mie resonator shifts shown in Fig. 1. Ultimately, then, uniform refractive-index tuning can be used to tune the optimal operating wavelength of a metalens. Such effects could be particularly useful for correcting efficiency reductions associated with fabrication or design errors.

II. CONCLUSION

In summary, we present a metalens design based on a single etch step into a high-index semiconductor. The design exploits a high-aspect-ratio, higher-order multipole resonator to achieve high focusing efficiencies over large NA values and focal lengths. We experimentally demonstrate the thermal tuning of InSb Mie resonators to extract a modal refractive-index change of 0.15 based on the spectral shifts of the MD resonance. Subsequently, we demonstrate that a continuous and uniform change in the refractive index of the metalens can actively tune the optimal operating wavelength, and in turn the focal length, due to chromatic dispersion. This result shows us that uniform thermal tuning of resonant semiconductor

meta-atoms can be used for tuning metasurface operating wavelengths, mirroring the chromatic dispersions inherent to the individual meta-atom Mie resonances.

ACKNOWLEDGMENTS

This work was supported by the Air Force Office of Scientific Research (Grant No. FA9550-16-1-0393). We also acknowledge support from the Centre for Scientific Computing from the CNSI and NSF Grant No. CNS-0960316. A part of this work was performed in the UCSB Nanofabrication Facility which is a part of the NSF funded National Nanotechnology Infrastructure Network.

P.P.I. and R.D. contributed equally to this work.

[1] Y. Kivshar and A. Miroshnichenko, Meta-optics with Mie resonances, Opt. Photonics News **28**, 24 (2017).

[2] A. I. Kuznetsov, A. E. Miroshnichenko, M. L. Brongersma, Y. S. Kivshar, and B. Luk'yanchuk, Optically resonant dielectric nanostructures, Science **354**, 2472 (2016).

[3] A. Arbabi, Y. Horie, M. Bagheri, and A. Faraon, Dielectric metasurfaces for complete control of phase and polarization with subwavelength spatial resolution and high transmission, Nat. Nanotechnol. **10**, 937 (2015).

[4] E. T. F. Rogers, J. Lindberg, T. Roy, S. Savo, J. E. Chad, M. R. Dennis, and N. I. Zheludev, A super-oscillatory lens optical microscope for subwavelength imaging, Nat. Mater. **11**, 432 (2012).

[5] D. Lin, P. Fan, E. Hasman, and M. L. Brongersma, Dielectric gradient metasurface optical elements, Science **345**, 298 (2014).

[6] D. Sell, J. Yang, S. Doshay, K. Zhang, and J. A. Fan, Visible light metasurfaces based on single-crystal silicon, ACS Photonics **3**, 1919 (2016).

[7] A. Arbabi, E. Arbabi, Y. Horie, S. M. Kamali, and A. Faraon, Planar metasurface retroreflector, Nat. Photonics **11**, 415 (2017).

[8] Q. Wang, E. T. F. Rogers, B. Gholipour, C.-M. Wang, G. Yuan, J. Teng, and N. I. Zheludev, Optically reconfigurable metasurfaces and photonic devices based on phase change materials, Nat. Photonics **10**, 60 (2015).

[9] N. A. Butakov, I. Valmianski, T. Lewi, C. Urban, Z. Ren, A. A. Mikhailovsky, S. D. Wilson, I. K. Schuller, and J. A. Schuller, Switchable plasmonic–dielectric resonators with metal–insulator transitions, ACS Photonics **5**, 371 (2018).

[10] T. Lewi, H. A. Evans, N. A. Butakov, and J. A. Schuller, Ultrawide thermo-optic tuning of PbTe meta-atoms, Nano Lett. **17**, 3940 (2017).

[11] M. Rahmani, L. Xu, A. E. Miroshnichenko, A. Komar, R. Camacho-Morales, H. Chen, Y. Zárate, S. Kruk, G. Zhang, D. N. Neshev, and Y. S. Kivshar, Reversible thermal tuning of all-dielectric metasurfaces, Adv. Funct. Mater. **27**, 1700580 (2017).

[12] P. P. Iyer, M. Pendharkar, C. J. Palmstrøm, and J. A. Schuller, Ultrawide thermal free-carrier tuning of dielectric antennas coupled to epsilon-near-zero substrates, Nat. Commun. **8**, 472 (2017).

[13] V. W. Brar, M. C. Sherrott, M. S. Jang, S. Kim, L. Kim, M. Choi, L. A. Sweatlock, and H. A. Atwater, Electronic modulation of infrared radiation in graphene plasmonic resonators, Nat. Commun. **6**, 7032 (2015).

[14] M. C. Sherrott, P. W. C. Hon, K. T. Fountaine, J. C. Garcia, S. M. Ponti, V. W. Brar, L. A. Sweatlock, and H. A. Atwater, Experimental demonstration of >230° phase modulation in gate-tunable graphene–gold reconfigurable mid-infrared metasurfaces, Nano Lett. **17**, 3027 (2017).

[15] Maxim R. Shcherbakov, Sheng Liu, Varvara V. Zubyuk, Aleksandr Vaskin, Polina P. Vabishchevich, Gordon Keeler, Thomas Pertsch, Tatyana V. Dolgova, Isabelle Staude, Igal Brener, and Andrey A. Fedyanin, Ultrafast all-optical tuning of direct-gap semiconductor metasurfaces, Nat. Commun. **8**, 17 (2017).

[16] P. P. Iyer, M. Pendharkar, and J. A. Schuller, Electrically reconfigurable metasurfaces using heterojunction resonators, Adv. Opt. Mater. **4**, 1582 (2016).

[17] T. Lewi, P. P. Iyer, N. A. Butakov, A. A. Mikhailovsky, and J. A. Schuller, Widely tunable infrared antennas using free carrier refraction, Nano Lett. **15**, 8188 (2015).

[18] P. P. Iyer, N. A. Butakov, and J. A. Schuller, Reconfigurable semiconductor phased-array metasurfaces, ACS Photonics **2**, 1077 (2015).

[19] H.-S. Ee and R. Agarwal, Tunable metasurface and flat optical zoom lens on a stretchable substrate, Nano Lett. **16**, 2818 (2016).

[20] S. Dong, K. Zhang, Z. Yu, and J. A. Fan, Electrochemically programmable plasmonic antennas, ACS Nano **10**, 6716 (2016).

[21] S. M. Kamali, E. Arbabi, A. Arbabi, Y. Horie, and A. Faraon, Highly tunable elastic dielectric metasurface lenses, Laser Photonics Rev. **10**, 1002 (2016).

[22] M. Decker, C. Kremers, A. Minovich, I. Staude, A. E. Miroshnichenko, D. Chigrin, D. N. Neshev, C. Jagadish, and Y. S. Kivshar, Electro-optical switching by liquid-crystal controlled metasurfaces, Opt. Express **21**, 8879 (2013).

[23] O. Buchnev, J. Y. Ou, M. Kaczmarek, N. I. Zheludev, and V. A. Fedotov, Electro-optical control in a plasmonic metamaterial hybridised with a liquid-crystal cell, Opt. Express **21**, 1633 (2013).

[24] T. Wipiejewski, D. B. Young, B. J. Thibeault, and L. A. Coldren, Thermal crosstalk in 4×4 vertical-cavity surface-emitting laser arrays, IEEE Photonics Technol. Lett. **8**, 980 (1996).

[25] I. Mathews, A. Abdullaev, S. Lei, R. Enright, M. J. Wallace, and J. F. Donegan, Reducing thermal crosstalk in ten-channel tunable slotted-laser arrays, Opt. Express **23**, 23380 (2015).

[26] E. Arbabi, A. Arbabi, S. M. Kamali, Y. Horie, and A. Faraon, Controlling the sign of chromatic dispersion in diffractive optics with dielectric metasurfaces, Optica **4**, 625 (2017).

[27] W. T. Chen, A. Y. Zhu, V. Sanjeev, M. Khorasaninejad, Z. Shi, E. Lee, and F. Capasso, A broadband achromatic metalens for focusing and imaging in the visible, Nat. Nanotechnol. **13**, 220 (2018).

[28] M. Khorasaninejad, Z. Shi, A. Y. Zhu, W. T. Chen, V. Sanjeev, A. Zaidi, and F. Capasso, Achromatic metalens over

60 nm bandwidth in the visible and metalens with reverse chromatic dispersion, Nano Lett. **17**, 1819 (2017).

[29] F. Aieta, M. A. Kats, P. Genevet, and F. Capasso, Multiwavelength achromatic metasurfaces by dispersive phase compensation, Science **347**, 1342 (2015).

[30] E. Arbabi, A. Arbabi, S. M. Kamali, Y. Horie, and A. Faraon, Multiwavelength polarization-insensitive lenses based on dielectric metasurfaces with meta-molecules, Optica **3**, 628 (2016).

[31] N. A. Butakov and J. A. Schuller, Designing multipolar resonances in dielectric metamaterials, Sci. Rep. **6**, 38487 (2016).

[32] C. F. Bohren and D. R. Huffman, *Absorption and Scattering of Light by Small Particles* (Wiley-VCH Verlag GmbH, Weinheim, Germany, 1998).

[33] G. D. Gillen, C. DiRocco, P. Powers, and S. Guha, Temperature-dependent refractive index measurements of wafer-shaped InAs and InSb, Appl. Opt. **47**, 164 (2008).

[34] G. Ghosh, *Handbook of Thermo-Optic Coefficients of Optical Materials with Applications* (Academic Press, San Diego, 1998).

[35] See Supplemental Material at http://link.aps.org/supplemental/10.1103/PhysRevApplied.10.044029 for additional information about the geometric dispersion of the resonators and the thermal free carrier effects.

[36] P. Y. Yu and M. Cardona, Temperature coefficient of the refractive index of diamond- and zinc-blende-type semiconductors, Phys. Rev. B **2**, 3193 (1970).

[37] FDTD Solutions Lumerical.com, (2015).

[38] M. Decker, I. Staude, M. Falkner, J. Dominguez, D. N. Neshev, I. Brener, T. Pertsch, and Y. S. Kivshar, High-efficiency dielectric Huygens' surfaces, Adv. Opt. Mater. **3**, 813 (2015).

[39] P. Lalanne and P. Chavel, Metalenses at visible wavelengths: past, present, perspectives, Laser Photonics Rev. **11**, 1600295 (2017).